J Arid Land (2025) 17(12): 1761–1784
doi: 10.1007/s40333-025-0114-7; CSTR: 32272.14.JAL.02501147

Science Press Springer-Verlag

Soil erosion and sediment connectivity variations in the Hantaichuan Watershed, northern Loess Plateau, China from 1995 to 2020

SHAN Rui[1], TIAN Peng[2], LU Ang[3], FAN Junjian[3], GUO Xiaoxue[1], ZHAO Yanbo[2], MU Xingmin[1,2], ZHAO Guangju[1,2,3*]

[1] State Key Laboratory of Soil and Water Conservation and Desertification Control, College of Soil and Water Conservation Science and Engineering, Northwest A&F University, Yangling 712100, China;
[2] State Key Laboratory of Water Disaster Prevention, Nanjing Hydraulic Research Institute, Nanjing 210029, China;
[3] Institute of Soil and Water Conservation, Chinese Academy of Sciences and Ministry of Water Resources, Yangling 712100, China

Abstract: Over the past six decades, the implementation of soil and water conservation measures has significantly reduced soil erosion and sediment yield on the Loess Plateau, China. However, while the overall reduction is well-documented, the dynamic interplay between soil erosion potential and sediment connectivity, specifically how they spatially covary under land use/cover changes, remains insufficiently understood. To address this gap, this study established a model framework by integrating the revised universal soil loss equation (RUSLE), index of connectivity (IC), and sediment delivery ratio (SDR) to evaluate the spatio-temporal variations in soil erosion and sediment yield in the Hantaichuan Watershed, northern Loess Plateau, China, from 1995 to 2020 and to estimate the effects of land use/cover changes and check dam construction on sediment yield. The results revealed that the soil erosion in the Hantaichuan Watershed decreased by 43.90% from 1995 to 2020 and the sediment yield decreased by 69.28% under the combination of land use/cover changes and check dam construction. The IC and soil erosion (IC–SE) map revealed both the coupling and decoupling covariation relationships between sediment connectivity and soil erosion. By 2020, areas with high connectivity and high erosion (I–E) covered only 18.67% of the watershed, while contributed more than 40.00% to the total erosion. The I–E zones were mainly located in the central part of the watershed where aeolian sands derived from the Hobq Desert are concentrated and were identified as critical areas for soil and water conservation. This study provides support for priority management of watershed conservation measures as well as a valuable reference for future studies.

Keywords: soil erosion; revised universal soil loss equation (RUSLE) model; index of connectivity (IC); sediment delivery ratio (SDR); land use/cover changes; check dam; Loess Plateau

Citation: SHAN Rui, TIAN Peng, LU Ang, FAN Junjian, GUO Xiaoxue, ZHAO Yanbo, MU Xingmin, ZHAO Guangju. 2025. Soil erosion and sediment connectivity variations in the Hantaichuan Watershed, northern Loess Plateau, China from 1995 to 2020. Journal of Arid Land, 17(12): 1761–1784. https://doi.org/10.1007/s40333-025-0114-7; https://cstr.cn/32276.14.JAL.02501147

1 Introduction

Soil erosion and sediment transport are critical processes within the Earth's surface system,

*Corresponding author: ZHAO Guangju (E-mail: gjzhao@nhri.cn)
Received 2025-07-02; revised 2025-11-15; accepted 2025-12-01

involving complex interactions among sediment generation, detachment, transport, and deposition (Bracken and Croke, 2007; Wuepper et al., 2020; Abebe et al., 2023; Zeng et al., 2025). These processes drive sediment transfer across diverse spatial and temporal scales, heavily regulated by land use patterns, climate conditions, and topography features (Baartman et al., 2013; Woznicki et al., 2020; Najafi et al., 2021). However, intensified anthropogenic activities and climate change have not only altered soil erosion rates but also significantly modified the efficiency of sediment delivery pathways, thereby triggering the implementation of extensive soil and water conservation measures in many erosion-prone regions. Therefore, quantifying spatio-temporal variations in soil erosion and sediment connectivity is essential for effective watershed management and for optimizing soil and water conservation strategies (Persichillo et al., 2018; Liu et al., 2024; Yang et al., 2025).

To address the challenge of sediment transport quantification and to evaluate the effectiveness of conservation measures, sediment connectivity has emerged as a critical parameter (Bracken and Croke, 2007). Sediment connectivity is defined as the degree of linkage that controls sediment transfer between different landscape components, from sources to sinks, and plays a key role in bridging the gap between estimates of hillslope erosion and catchment sediment yield (Bracken and Croke, 2007; Stephens et al., 2021; Zanandrea et al., 2021; Hao et al., 2022; Bhattacharya et al., 2024). Numerous methods for estimating sediment connectivity have been established (Chen et al., 2021; Tang et al., 2021; Liu et al., 2022; Liu et al., 2025). Early approaches include field observations, index methods, graph theoretic analyses, and tracer techniques (Vigiak et al., 2016; Abebe et al., 2023). Among these, the index of connectivity (IC) proposed by Borselli et al. (2008) has become the most widely adopted approach because of its flexibility and clear physical basis. For instance, Cavalli et al. (2013) advanced IC by incorporating a roughness index (RI) derived from the topography, thereby increasing the ability of this index to characterize sediment pathways in small watersheds. López-Vicente et al. (2013) combined IC with the revised Morgan-Morgan-Finney (RMMF) model to evaluate the impacts of different land use scenarios on sediment delivery dynamics. Hao et al. (2022) explored erosion-connectivity relationships at the event scale via the modified universal soil loss equation (MUSLE) combined with IC. The adaptability of IC framework makes it particularly effective for assessing landscapes undergoing significant anthropogenic transformation, such as the Loess Plateau, China. On the Loess Plateau, extensive soil and water conservation measures, including vegetation restoration, land use changes, and the construction of check dams, have dramatically altered flow paths, thereby affecting changes in sediment connectivity. In previous studies, Zhao et al. (2020) used the IC–revised universal soil loss equation (RUSLE) framework in the Yanhe River Catchment on the Loess Plateau to quantify reductions in sediment yield attributable to vegetation restoration and check dam construction, whereas Guo et al. (2023) developed an approach that combines IC with an impedance factor derived from surface roughness to characterize changes in sediment connectivity in the same catchment. While these studies have demonstrated the overall impact of conservation measures, the long-term evolution of the covariation between soil erosion potential and sediment connectivity under continued ecological restoration and large-scale check-dam construction on the Loess Plateau remains insufficiently understood. Alao, a key challenge remains in clarifying the covariation between soil erosion potential and sediment connectivity, which is crucial for identifying not only erosion hotspots but also persistent or emerging critical source areas that actively contribute to the sediment yield at the catchment outlet.

An effective approach to investigate the interplay between erosion and sediment transport is to explicitly link gross erosion estimates with the sediment delivery ratio (SDR). SDR, defined as the ratio of the sediment yield of the watershed to the total gross erosion, serves as a crucial indicator of the overall transport efficiency of a basin (Borselli et al., 2008). RUSLE is a widely applied empirical model for estimating gross erosion. Owing to its robust structure and relatively straightforward data requirements, RUSLE is particularly effective for assessing the long-term

spatio-temporal dynamics of soil erosion under varying land use and management scenarios (Wischmeier and Smith, 1978; Renard et al., 1997). However, RUSLE captures only potential soil detachment, although a substantial portion of eroded sediment is often redeposited within slopes or channels or behind structures such as check dams. SDR bridges this gap by linking the potential erosion with the actual sediment delivery. Recent advancements have demonstrated that SDR is not a static catchment-wide metric but can be spatially estimated through its functional relationship with sediment connectivity. Empirical studies have increasingly demonstrated a sigmoidal relationship between IC and SDR, allowing spatially distributed IC values to inform SDR estimates (Hamel et al., 2017; Zhao et al., 2020; Liu et al., 2021). Therefore, by combining an empirical soil erosion model RUSLE with a connectivity-driven SDR, an integrated framework is established to assess sediment yield processes over a long-time series. This framework provides the necessary spatial information on both erosion potential and sediment transport efficiency, enabling a detailed analysis of their covariation.

Accordingly, this research focused on the Hantaichuan Watershed, a representative watershed on the northern Loess Plateau, characterized by a steep topography and widespread fragile Pisha sandstone. In the past decades, a series of soil and water conservation measures have been implemented in this watershed, including large-scale vegetation restoration and the construction of check dams, which have led to substantial changes in land surface and have consequently altered sediment yield and sediment connectivity. The specific objectives of this study are to: (1) estimate the spatio-temporal dynamics of soil erosion and sediment yield in the Hantaichuan Watershed from 1995 to 2020 using an integrated framework that combines RUSLE model with IC and SDR; (2) evaluate the impacts of land use/cover change and check dams construction on soil erosion and sediment yield; and (3) analyze the covariation between sediment connectivity and soil erosion with respect to the evolution of critical sediment source areas. This paper offers a novel perspective for targeted watershed management and optimization of soil and water conservation strategies in highly human-impacted loess catchments.

2 Materials and methods

2.1 Study area and data collection

The Hantaichuan Watershed (39°50′–40°29′N, 109°45′–110°41′E) is located in the upper reaches of the Yellow River Basin within Ordos City, Inner Mongolia Autonomous Region, China, and covers a total area of 874.70 km^2. The Xiangshawan Hydrological Station is located in the downstream of the tributary, with a controlled catchment area of 826.00 km^2. The Hantaichuan Watershed is a representative tributary of the Ten Kongduis (ephemeral gully systems derived from Mongolian hydrologic terminology) on the Inner Mongolia Plateau, crossing the Hobq Desert before entering the Yellow River (Fig. 1a). The dominant soil types in the watershed include weathered sandstone (Pisha sandstone), loess, and sandy soils (Fan et al., 2024; Zhang, 2024). Hydrological records (1980–2022) reveal that the watershed is characterized as a typical arid area encompassing intermittent river flooding conditions, with dry conditions prevailing throughout 70.00% of the channel network annually. The average annual precipitation is 350 mm, which is mostly concentrated between July and October, primarily in a form of heavy rainfall events (Wang et al., 2018). Historical studies have shown that regional soil erosion is extremely serious owing to the effects of fragile ecological environments and extensive agricultural activities (Yang and Shi, 2018; Zhao, 2023; Sheng et al., 2025). Since the 1990s, ecological restoration and management measures have been implemented in the watershed, and soil erosion has been effectively alleviated.

We delineated the Hantaichuan Watershed into 24 sub-basins using the automatic watershed delineation procedure in the Soil and Water Assessment Tool (SWAT) (United States Department of Agriculture (USDA) Agricultural Research Service, Temple, USA). The digital elevation model (DEM) was hydrologically preprocessed (sink filling and generation of

flow-direction and flow-accumulation grids), and a minimum drainage area threshold was applied to the flow-accumulation grid to define the stream network and sub-basin outlets so that the simulated channels matched the observed river network. The watershed outlet was fixed at the Xiangshawan Hydrological Station and additional outlets were placed at major tributary confluences, resulting in 24 hydrologically sub-basins, a delineation approach widely used in SWAT applications for runoff and sediment simulations (Fig. 1b) (Arnold et al., 1998). The dataset included observed sediment, DEM, precipitation, vegetation cover, land use, and soil data. All the data sources are listed in Table 1. We used the DEM data to calculate the slope length and steepness factor, and the soil data to calculate soil erodibility. A time series normalized difference vegetation index (NDVI) dataset derived from Advanced Very High Resolution Radiometer (AVHRR) and Moderate Resolution Imaging Spectroradiometer (MODIS) sensors was used after consistency correction and downscaling (Pinzon et al., 2023). The applicability of NDVI dataset to large-scale watersheds has been verified (Zhang et al., 2016), offering reliable support for assessing the impacts of ecological restoration.

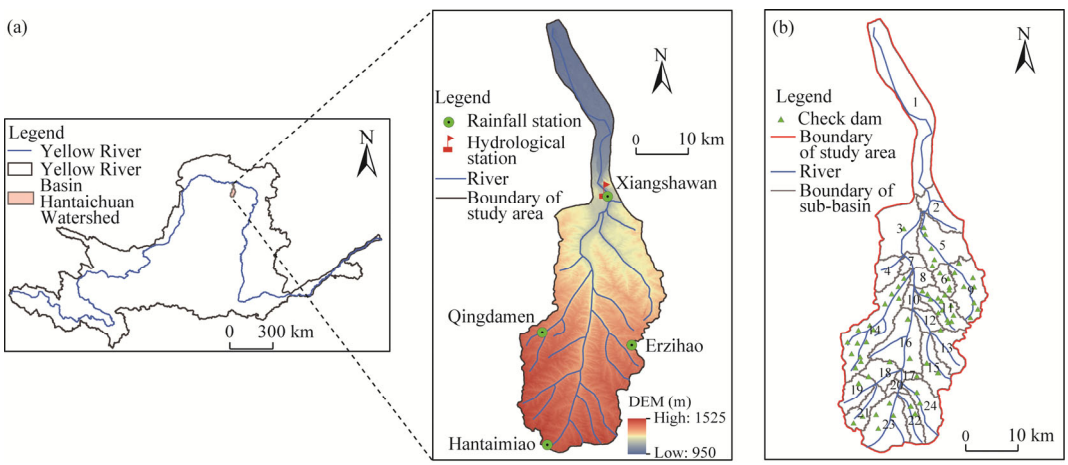

Fig. 1 Location (a) and sub-basin zoning (b) of the Hantaichuan Watershed. DEM, digital elevation model. The numbers in Figure 1b are the serial numbers of sub-basins.

2.2 Model framework

The integrated modeling framework was implemented by four main steps: (1) soil erosion modeling by using RUSLE model; (2) calculating IC and SDR; (3) analyzing the relationship between IC and soil erosion (IC–SE) at the sub-basin scale; and (4) validating the model outputs (Fig. 2).

2.2.1 RUSLE model

Soil erosion involves the detachment and transport processes of surface soil within a watershed caused by external forces. In this study, RUSLE model was applied to quantify soil erosion (Renard et al., 1997; Ganasri and Ramesh, 2016; Thapa, 2020). RUSLE model can be expressed as follows:

$$A = R \times K \times L \times S \times C \times P, \quad (1)$$

where A is the erosion modulus (t/(km^2·a)); R is the rainfall erosivity factor (MJ·mm/(km^2·h·a)); K is the soil erodibility factor (t·h/(MJ·mm)); L is the slope length factor; S is the slope steepness factor; C is the cover management factor; and P is the soil conservation practice factor.

The rainfall erosivity factor reflects the potential capacity of rainfall to cause soil erosion. We calculated the values of rainfall erosivity factor at each rainfall station via the erosive daily rainfall method proposed by Zhang and Fu (2003), which has been widely applied on the Loess Plateau (Luo, 2022; Guo et al., 2023; Zhao, 2023; Liu, 2024), followed by spatial interpolation across the basin to obtain the mean annual rainfall erosivity. The calculations are as follows:

Table 1 Description and source of data

Dataset	Data type	Period	Resolution	Description	Data source
DEM (m)	Raster	2020	30 m	ASTER DEM	Geospatial Data Cloud (http://www.gscloud.cn/)
precipitation (mm)	Time series	1995–2020	-	Daily precipitation data of the Hantaichuan Watershed from four rainfall stations (Erzihao, Qingdamen, Xiangshawan, and Hantaimiao)	Ministry of Water Resources of the People's Republic of China (1995–2020)
Sediment (kg/m^3)	Time series	1995–2020	-	Suspended sediment concentrations at the Xiangshawan Hydrological Station	Ministry of Water Resources of the People's Republic of China (1995–2020)
NDVI	Raster	1995, 2000, 2005, 2010, 2015, and 2020	100 m	NDVI data were obtained from AVHRR and MODIS NDVI products.	Research Center for Digital Mountain and Remote Sensing Application, Institute of Mountain Hazards and Environment, Chinese Academy of Sciences (CAS) (http://digitalmountain.imde.ac.cn)
Land use	Raster	1995, 2000, 2005, 2010, 2015, and 2020	30 m	Land use data were classified into six categories: arable land, forest land, grassland, water body, construction land, and bare land.	Geographical Information Monitoring Cloud Platform (http://www.dsac.cn/)
Soil	Raster	2020	1:1,000,000	Soil type map and the information on related soil properties	National Earth System Science Data Center, National Science & Technology Infrastructure (http://loess.geodata.cn)

Note: DEM, digital elevation model; ASTER, Advanced Spaceborne Thermal Emission and Reflection Radiometer; NDVI, normalized difference vegetation index; AVHRR, Advanced Very High Resolution Radiometer; MODIS, Moderate Resolution Imaging Spectroradiometer; -, no resolution.

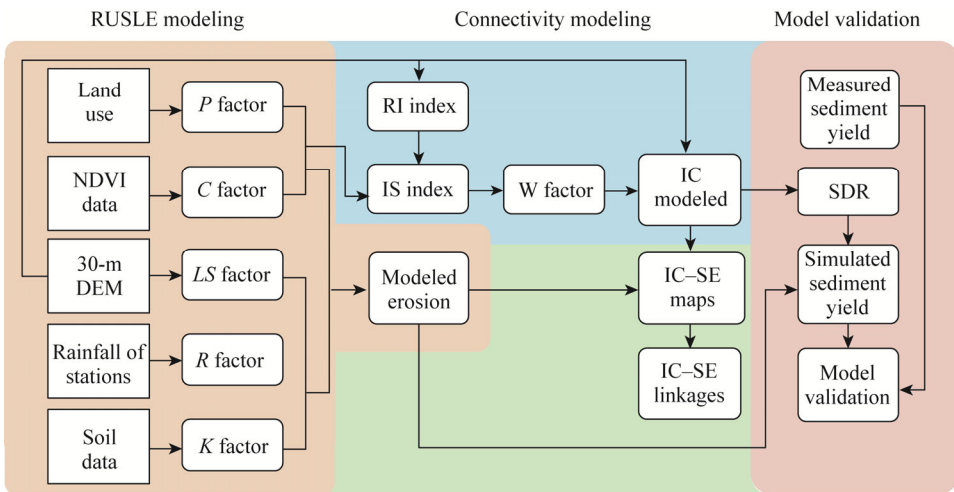

Fig. 2 Workflow of this study. *P* factor, soil conservation practice factor; *C* factor, cover management factor; *LS* factor, the combination of is the slope length and slope steepness factors; *R* factor, rainfall erosivity factor; *K* factor, soil erodibility factor; NDVI, normalized difference vegetation index; RI, roughness index; IC, index of connectivity; IC–SE, index of connectivity–soil erosion; SDR, sediment delivery ratio. IS index is the impedance index, reflecting the combined effects of topography, vegetation, and soil and water conservation measures; and the W factor is the impedance factor, reflecting the ability of vegetation and topography to resist sediment movement.

$$M = a\sum_{j=1}^{h}(D_j)^{\beta}, \tag{2}$$

$$a = 21.586\beta^{7.1891}, \tag{3}$$

$$\beta = 0.8363 + \frac{18.177}{T_{d12}} + \frac{24.455}{T_{y12}}, \tag{4}$$

where M is the half-month rainfall erosivity (MJ·mm/(km^2·h·a)); D_j is the daily rainfall on erosive day j (daily rainfall ≥12 mm) (mm); h is the number of days with a daily rainfall ≥12 mm; T_{d12} and T_{y12} are the mean rainfall on erosive days (daily rainfall ≥12 mm) and the mean annual rainfall, respectively (mm); and α and β are the empirical parameters determined by regional rainfall characteristics. We spatially interpolated the rainfall erosivity values through inverse distance weighting (IDW) method to derive the rainfall erosivity factor distribution across the watershed.

The soil erodibility factor reflects the susceptibility of soil to erosion by rainfall and surface flow and can be expressed follows (Sun et al., 2014):

$$K = 0.1317 \times \left\{0.2 + 0.3\exp\left[-0.0256\mathrm{SAN}\frac{(1-\mathrm{SIL})}{100}\right]\right\} \times \left(\frac{\mathrm{SIL}}{\mathrm{CLA+SIL}}\right)^{0.3} \times \left(1.0 - \frac{0.25\mathrm{SOC}}{\mathrm{SOC+exp(3.72-2.92SOC)}}\right) \times \left(1.0 - \frac{0.7\mathrm{SNI}}{\mathrm{SNI+exp(-5.51+22.9SNI)}}\right), \tag{5}$$

$$\mathrm{SNI} = 1 - \frac{\mathrm{SAN}}{100}, \tag{6}$$

where SAN, SIL, and CLA are the proportions of sandy, silty, and clay (%), respectively; SOC is the organic carbon content (%); and SNI is an auxiliary soil structure index.

The slope length factor and slope steepness factor are derived from DEM. The slope length exponent (m) varies according to the slope gradient (Fu et al., 2011):

$$L = \left(\frac{\lambda}{22.13}\right)^m \begin{cases} m = 0.5 & (\theta \geq 3.0°) \\ m = 0.4 & (1.5° \leq \theta < 3.0°) \\ m = 0.3 & (0.5° \leq \theta < 1.5°) \\ m = 0.2 & (\theta < 0.5°) \end{cases}, \tag{7}$$

$$S = \begin{cases} 10.8\sin\theta + 0.03 & (\theta < 5.0°) \\ 16.8\sin\theta - 0.05 & (5.0° \leq \theta < 14.0°) \\ 21.91\sin\theta - 0.96 & (\theta \geq 14.0°) \end{cases}, \tag{8}$$

where λ is the slope length (m); and θ is the slope angle (°).

The cover management factor represents the influence of vegetation and tillage on soil erosion resistance. In the method developed by Cai et al. (2000), which has been widely applied in the study of the Loess Plateau (Luo, 2022; Zhao, 2023; Liu, 2024; Min et al., 2024). We calculated the vegetation coverage (f) using NDVI and then converted to cover management factor. The calculations are as follows:

$$f = \frac{\mathrm{NDVI} - \mathrm{NDVI}_{\min}}{\mathrm{NDVI}_{\max} - \mathrm{NDVI}_{\min}}, \tag{9}$$

$$C = \begin{cases} 1 & (f \leq 0.096) \\ 0.6508 - 0.3436\log_{10} f & (0.096 < f \leq 0.783) \\ 0 & (f \geq 0.783) \end{cases}, \tag{10}$$

where $\mathrm{NDVI}_{\max}$ is the maximum NDVI value with a cumulative probability of 95.00% (vegetation vigorous period); and $\mathrm{NDVI}_{\min}$ is the minimum NDVI value of bare land (benchmark reference).

The soil conservation practice factor accounts for soil conservation measures that reduce

erosion potential. Referring to Guo et al. (2023) and Zhao (2023), we assigned soil conservation practice factor as follows: forest land (P=0.70), grassland (P=0.90), water body (P=0.00), bare land (P=1.00), arable land (P=0.35), and construction land (P=0.00).

After the calculation of erosion modulus, via the use of the Soil Erosion Classification and Grading Standard (SL190-2007) (Ministry of Water Resources of the People's Republic of China, 2008), we classified erosion into five levels: micro (<1000.00 t/(km^2·a)), slight (1000.00–2500.00 t/(km^2·a)), moderate (2500.00–5000.00 t/(km^2·a)), strong (5000.00–8000.00 t/(km^2·a)), and high (8000.00–15,000.00 t/(km^2·a)) erosion.

2.2.2 IC

IC reflects the potential for sediment transfer from source to sink. With the basin outlet defined as the final sediment sink, we calculated IC as follows (Borselli et al., 2008):

$$\mathrm{IC}=\log_{10}\frac{D_{\mathrm{up}}}{D_{\mathrm{dn}}}=\log\left(\frac{\overline{W}\times\overline{S}\times\sqrt{Z}}{\sum_{i=1}^{u}\frac{d_i}{W_iS_i}}\right), \tag{11}$$

where D_{up} and D_{dn} are the upslope and downslope components, respectively; $\overline{W}$ is the average weighting factor of the upslope area; $\overline{S}$ is the average slope gradient of the upslope contributing area; Z is the upslope contributing area (m^2); u is the number of cells along the steepest downslope flow path; d_i is the length of the i^{th} cell along the steepest downslope path to the sink (m); W_i is the impedance factor of the i^{th} cell, computed by Equations 12 and 13; and S_i is the slope gradient of the i^{th} cell.

In this study, the impedance factor reflects the ability of vegetation and topography to resist sediment movement. Several algorithms have been developed for calculating the impedance factor. While some studies utilized the cover management factor from RUSLE model (Zhao et al., 2020) to quantify this factor, others adopted hydraulic or morphometric metrics, such as surface roughness (Michalek et al., 2021), the runoff coefficient (Millares-Valenzuela et al., 2022), and the Manning coefficient (Zanandrea et al., 2019). In this study, we computed an impedance index using RI, cover management factor, and soil conservation practice factor, following the methods validated by Guo et al. (2023) for the Loess Plateau. The calculations are as follows:

$$\mathrm{IS}=\mathrm{RI}+C\times P, \tag{12}$$

$$W=1-\frac{\mathrm{IS}}{\mathrm{IS}_{\max}}, \tag{13}$$

where W is the impedance factor; IS is an impedance index that combines the effects of topography, vegetation, and soil and water conservation measures; and $\mathrm{IS}_{\max}$ is the maximum IS in the study area.

2.2.3 SDR

SDR represents the proportion of the total sediment that reaches the watershed outlet relative to the total soil erosion. Vigiak et al. (2012) developed a logistic model that links SDR to sediment connectivity, which has been widely used on the Loess Plateau (Zhao et al., 2020; Liu et al., 2021; Guo et al., 2023). The relationship is defined as follows:

$$\mathrm{SDR}_i=\frac{\mathrm{SDR}_{\max}}{1+\exp\left(\frac{\mathrm{IC}_0-\mathrm{IC}_i}{l}\right)}, \tag{14}$$

where SDR_i is the sediment delivery ratio in the i^{th} cell; $\mathrm{SDR}_{\max}$ is the maximum theoretical SDR with a range of 0–1, of which $\mathrm{SDR}_{\max}$=1 reflects high-intensity sediment transport (Zhao et al., 2020); IC_i is the connectivity index of the i^{th} cell; IC_0 is a calibration connectivity index, set to 0.5; and l is a calibration parameter, set to 2.0. These parameters collectively determine the

sigmoidal relationship between SDR and IC.

The total sediment yield of a given catchment can be calculated from the soil erosion modulus and SDR values (Jain and Kothyari, 2000):

$$\mathrm{SY} = \sum_{i=1}^{N} A_i \times \mathrm{SDR}_i , \tag{15}$$

where SY is the sediment yield (t/(km^2·a)); A_i is the soil erosion modulus of the i^{th} cell (t/(km^2·a)); and N is the total number of cells within the watershed.

2.2.4 Sediment delivery in channels

Owing to the widespread distribution of check dams in the study area, their trapping efficiencies can be derived from structural characteristics as follows (Brune, 1953):

$$\mathrm{TE} = 1 - \frac{1}{1 + 0.0021 D \dfrac{V}{F}} , \tag{16}$$

where TE is the trapping efficiency of check dams, ranging from 0 to 1; V is the sediment storage capacity (m^3); F is the controlled watershed area (km^2); and D is an empirical coefficient that depends on factors such as sediment storage capacity, control area, annual runoff, and sediment texture. The value of D typically ranges from 0.046 to 1.000; following the approach of Zhao et al. (2017), we set the value of D to 0.100 in this study to represent the average trapping condition of check dams in the Hantaichuan Watershed.

2.2.5 Sediment connectivity and erosion relationship map

In this study, we created a IC–SE relationship diagram through the following steps: (1) data preparation: spatial datasets of soil erosion and sediment connectivity for the Hantaichuan Watershed from 1995 to 2020 were compiled via the use of RUSLE model and IC; (2) covariation analysis: the relationship between IC (x-axis) and soil erosion (y-axis) was analyzed at the sub-basin level; and (3) classification of IC–SE patterns: the Jenks natural breakpoint method (Jenks, 1967) was applied to divide the dual-axis thresholds and to delineate four distinct IC–SE covariation classifications. Notably, zones with high sediment connectivity and high erosion (I–E) were classified as priority management areas; those with high connectivity and low erosion (I–e) were classified as connectivity-sensitive areas; those with low connectivity and high erosion (i–E) were classified as potential erosion risk areas; and those with low connectivity and low erosion (i–e) were classified as ecologically stable areas. For a comprehensive overview of the procedures, refer to Michalek et al. (2021), who provide detailed information.

2.3 Model validation

Validation of RUSLE model is challenging because it aims to primarily estimate hillslope soil erosion, whereas direct field measurements of soil erosion are often limited and difficult to obtain (Guo et al., 2023). To address this limitation, we integrated RUSLE model with SDR to estimate the total sediment yield at the watershed scale. We validated the model by comparing the simulated annual sediment yields with the observed data from the Xiangshawan Hydrological Station (located at the outlet of the Hantaichuan Watershed). We used the coefficient of determination (R^2) to assess the linear relationship between the simulated and observed values. The overall predictive accuracy of the model was evaluated with the Nash-Sutcliffe efficiency coefficient (NSE).

$$R^2 = \frac{\left[\sum_{i=1}^{n}\left(Q_{m,i} - \overline{Q_m}\right)\left(Q_{s,i} - \overline{Q_s}\right)\right]^2}{\sum_{i=1}^{n}\left(Q_{m,i} - \overline{Q_m}\right)^2 \sum_{i=1}^{n}\left(Q_{s,i} - \overline{Q_s}\right)^2} , \tag{17}$$

$$\mathrm{NSE} = 1 - \frac{\sum_{i=1}^{n}(Q_{m,i} - Q_{s,i})^2}{\sum_{i=1}^{n}(Q_{\mathrm{m},i} - \overline{Q_m})^2}, \tag{18}$$

where $Q_{m,i}$ and $Q_{s,i}$ are the measured and simulated values of the i^{th} sample, respectively; $\overline{Q_m}$ and $\overline{Q_s}$ are the mean measured and simulated values, respectively; and n is the number of years.

3 Results

3.1 Erosion modeling

3.1.1 Erosion factor analysis

Based on long-term rainfall data, the rainfall erosivity factor exhibited significant spatial heterogeneity (Fig. 3). Although calculated as a multi-year mean and treated as temporally invariant for the RUSLE simulations to represent the long-term climatic rainfall erosivity regime, the factor showed distinct spatial patterns. Spatially, higher rainfall erosivity factor values were concentrated in the northern part of the watershed, and they gradually decreased from north to south across the watershed. During the study period, the soil erodibility factor averaged approximately 0.20 t·h/(MJ·mm) and demonstrated clear spatial variation, with higher values in the northern part of the watershed and lower values in the central and southern regions. The slope length factor values ranged from 1.06 to 1.66, whereas the slope steepness factor was relatively high in the southern part of the watershed, particularly on the steeper slopes between gullies, reaching 16.26.

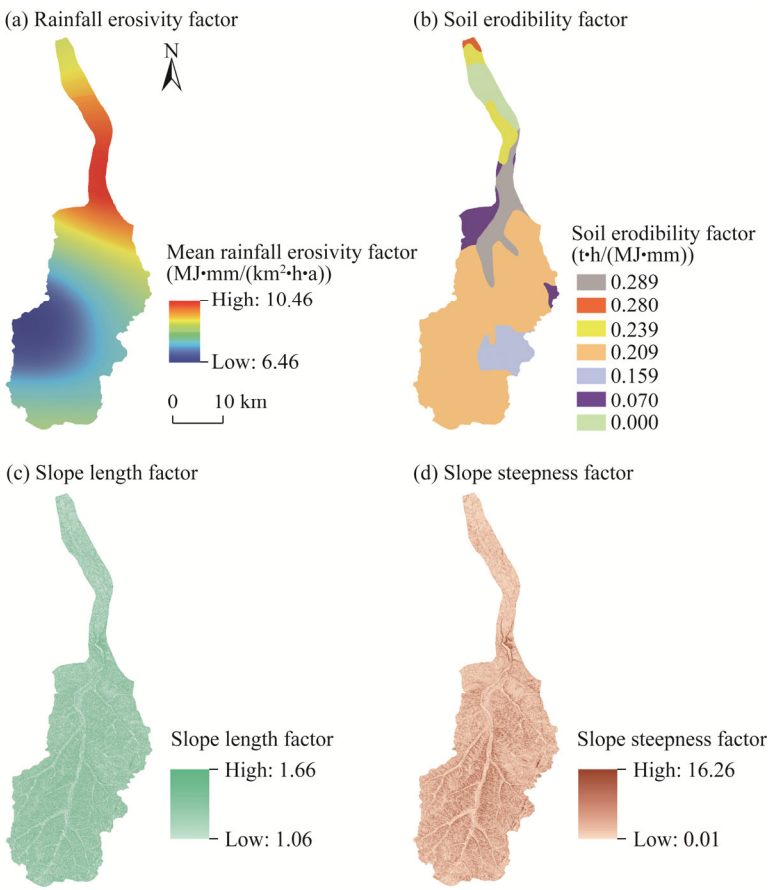

Fig. 3 Spatial distribution of soil erosion factors. (a), multi-year mean rainfall erosivity factor of 1995–2020; (b), soil erodibility factor; (c), slope length factor; (d), slope steepness factor.

3.1.2 Changes in soil conservation practice factor and cover management factor

From 1995 to 2020, the main land use type in the Hantaichuan Watershed was grassland, accounting for more than 70.00% of the watershed, followed by arable land and bare land, each occupying less than 12.00% of the watershed (Table 2; Fig. 4). From 1995 to 2020, the area of bare land significantly decreased, whereas forest land and construction land expanded notably, indicating the combined effect of vegetation restoration and urbanization. Water body showed the smallest change, remaining relatively stable at approximately 41.00 km^2 throughout the study period. In contrast, construction land increased the most, expanding by 51.22 km^2, reflecting the rapid process of urbanization in the basin from 1995 to 2020. The soil conservation practice factor was determined by land use, which was dominated by extensive high-value areas throughout the watershed, whereas low-value areas were confined to scattered patches of construction land and water body (Fig. 5). From 1995 to 2020, the extent of high soil conservation practice factor zones gradually increased.

The spatial distribution of the cover management factor values decreased notably from 0.88 in 1995 to 0.74 in 2020 (Fig. 6). In 1995, the cover management values were lower in the northern part of the watershed and higher in the central and southern regions, as influenced by the implementation of vegetation restoration and other management measures. By 2020, cover management values had generally decreased across most central and southern sub-basins, mainly owing to large-scale vegetation restoration, although some sub-basins (e.g., 14, 16, and 18) still exhibited relatively high values.

Table 2 Land use change in the Hantaichuan Watershed

Year	Arable land		Grassland		Forest land		Water body		Construction land		Bare land	
	Area (km^2)	Percentage (%)	Area (km^2)	Percentage (%)	Area (km^2)	Percentage (%)	Area (km^2)	Percentage (%)	Area (km^2)	Percentage (%)	Area (km^2)	Percentage (%)
1995	80.65	9.22	629.43	71.96	15.28	1.75	41.74	4.77	8.64	0.99	98.96	11.31
2000	79.72	9.11	635.50	72.65	31.84	3.64	41.87	4.79	8.43	0.96	77.34	8.85
2005	74.78	8.55	631.90	72.24	31.07	3.55	41.74	4.77	21.60	2.47	73.61	8.42
2010	73.67	8.42	630.72	72.11	30.75	3.52	41.73	4.77	26.91	3.08	70.92	8.10
2015	68.79	7.86	634.08	72.49	30.90	3.53	41.44	4.74	42.95	4.91	56.54	6.47
2020	60.06	6.87	636.75	72.80	31.49	3.60	41.25	4.72	59.86	6.84	45.29	5.17

3.1.3 Spatio-temporal distribution of soil erosion

The distribution of soil erosion in the watershed revealed significant spatial heterogeneity (Fig. 7). The most severe erosion was concentrated in the central part of the watershed, particularly within sub-basins 2, 3, and 5–9, whereas both the northern and the southern sub-basins experienced relatively low erosion intensity. Sub-basin 2 consistently remained the primary erosion hotspot throughout the study period. From 1995 to 1999, the erosion modulus decreased rapidly from 2261.51 to 825.27 t/(km^2·a), a reduction of 63.51%. A notable increase occurred during 2000–2004, with the average erosion modulus increasing to 1285.84 t/(km^2·a). Thereafter, erosion decreased slowly during 2005–2020 and stabilized at approximately 1268.65 t/(km^2·a), with the most significant decreases in the central and southern parts of the watershed. Overall, the basin-wide mean erosion modulus declined by 43.90% from 1995 to 2020. Notably, sub-basin 2 still maintained a high erosion intensity (>2500.00 t/(km^2·a)).

From 1995 to 2020, micro erosion (<1000.00 t/(km^2·a)) and slight erosion (1000.00–2500.00 t/(km^2·a)) fluctuated but increased overall, accounting for approximately 96.20% of the watershed area in 2020. In contrast, moderate (2500.00–5000.00 t/(km^2·a)) and strong (5000.00–8000.00 t/(km^2·a)) erosion decreased in area and stabilized after 2000, of which, moderate erosion area disappeared after 2000. Notably, no extremely high erosion (8000.00–15,000.00 t/(km^2·a)) was observed. Erosion hotspots progressively contracted and became concentrated in the central sub-basins by the end of the study period.

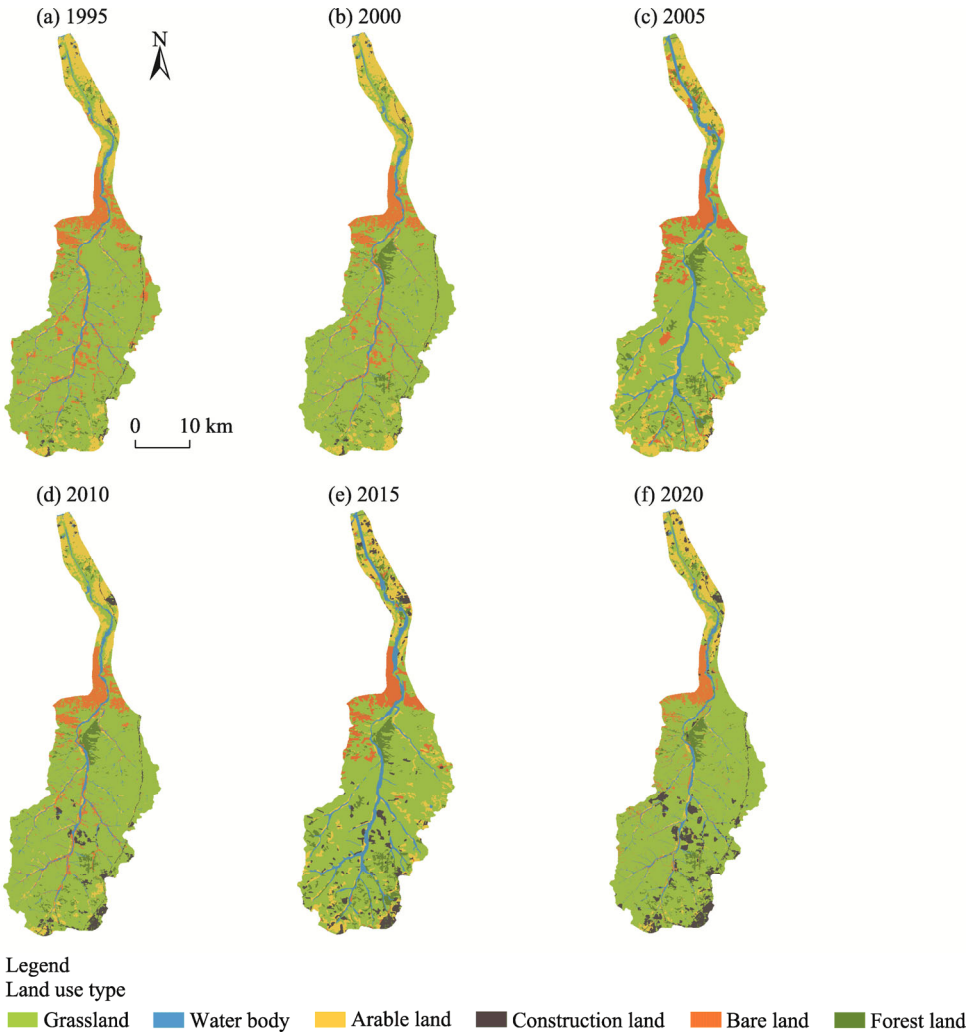

Fig. 4 Spatial distribution of land use type in the Hantaichuan Watershed in 1995 (a), 2000 (b), 2005 (c), 2010 (d), 2015 (e), and 2020 (f)

3.2 Spatio-temporal variability in sediment connectivity and SDR

Sediment connectivity in the Hantaichuan Watershed exhibited significant spatial heterogeneity (Fig. 8). Low IC values were primarily concentrated in the northern (sub-basin 1), eastern (sub-basins 6, 9, and 11), and southern regions (sub-basins 14, and 21–24), forming a pattern that largely coincided with areas of dense check-dam construction (Fig. 1b). This spatial correspondence suggested that soil and water conservation engineering has contributed to reducing sediment connectivity by trapping runoff and sediment. From 1995 to 2020, the basin-wide mean IC showed minor fluctuations in the late 1990s, followed by an overall decline, which was consistent with the progressive decrease in the cover management factor (Fig. 8).

The spatial pattern of SDR closely mirrored that of IC (Fig. 9). In 1995, SDR values were highest in the central part of the watershed, particularly in sub-basin 2 with value of 0.50, and gradually decreased toward the southern reach. By 2020, SDR values across the watershed had notably decreased, with most southern sub-basins showing values less than 0.20 (e.g., sub-basins 19–24). The temporal evolution showed distinct stage characteristics. During the high-value fluctuation period (1995–1999), the basin-wide mean SDR reached 0.37, followed by a considerable decrease to 0.19 from 2000 to 2020.

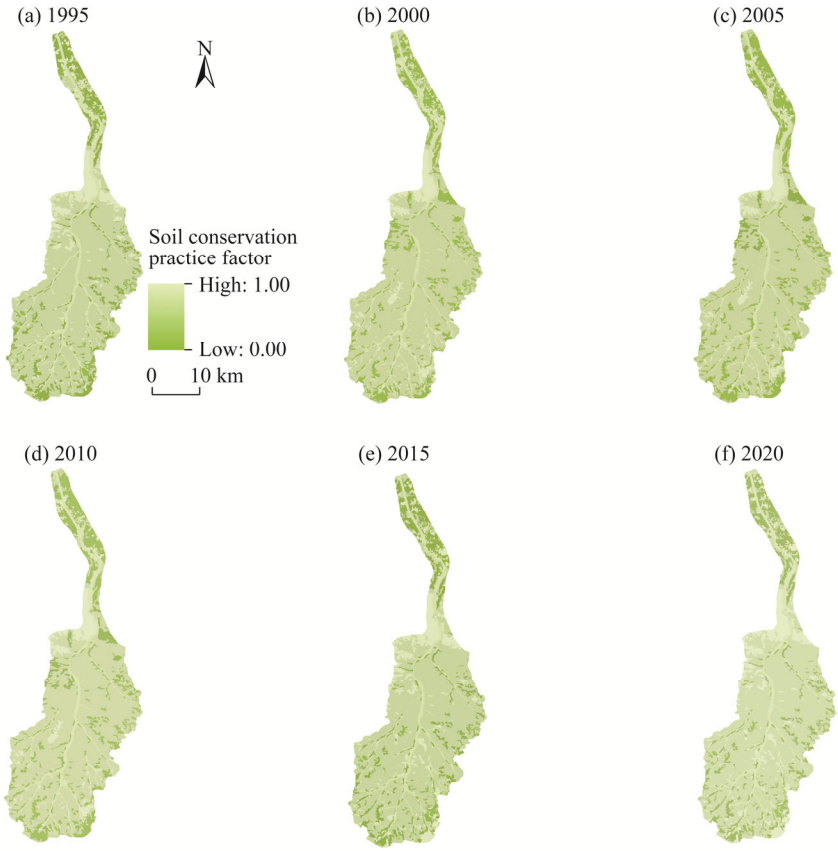

Fig. 5 Spatial distribution of soil conservation practice factor in the Hantaichuan Watershed in 1995 (a), 2000 (b), 2005 (c), 2010 (d), 2015 (e), and 2020 (f)

3.3 Changes in sediment yield and model validation

We combined IC and SDR with RUSLE model to estimate sediment yield in the Hantaichuan Watershed. As shown in Figure 10, sediment yield decreased from 693.30 t/(km^2·a) in 1995 to 212.99 t/(km^2·a) in 2020 (a reduction of 69.28%), owing to the combined effects of check dams and land use/cover changes. When only considering the land use/cover changes (Fig. 11), sediment yield in the central sub-basins was generally higher than in the southern and northern parts of the watershed. Temporally, the basin-wide mean annual sediment yield declined from 783.76 to 285.27 t/(km^2·a), a reduction of 63.60%, while the central part of the watershed, particularly sub-basins 2, 3, 5, and 7, consistently remained the key sediment-yield hotspot. A comparison of Figures 10 and 11 further indicated that the inclusion of check dam trapping led to an additional reduction in sediment yield, especially in the central (e.g., sub-basins 6, 9, and 11) and southern sub-basins (e.g., sub-basins 14 and 23) where check dams are densely distributed.

The result of the validation of an integrated modeling framework was satisfactory. The correlation between the simulated and observed sediment yields (R^2=0.64) confirmed good model reliability (Fig. 12). However, NSE value was 0.56, indicating acceptable model performance. Compared with the observations, the model slightly underestimated the sediment yield in 1996 and overestimated it after 2010, which can be partly attributed to uncertainties arising from limitations in the input data and the simplified static representation of check dam trapping efficiency within the modeling framework.

3.4 Covariation between sediment connectivity and soil erosion

The IC–SE map revealed dynamic covariation between sediment connectivity and soil erosion in the Hantaichuan Watershed (Fig. 13). From 1995 to 2020, coupled IC–SE relationships (I–E and

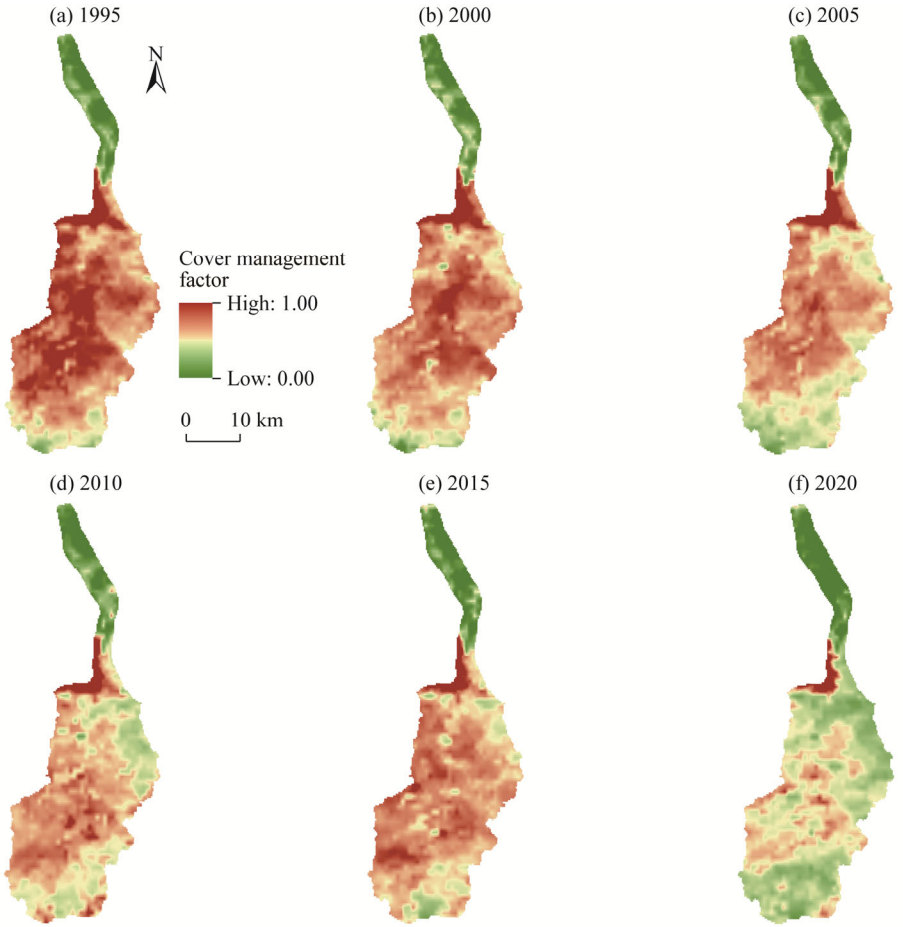

Fig. 6 Spatial distribution of cover management factor in the Hantaichuan Watershed in 1995 (a), 2000 (b), 2005 (c), 2010 (d), 2015 (e), and 2020 (f)

i–e quadrants) occupied 60.20% of the watershed area and contributed 71.30% of total erosion, whereas decoupled relationships (I–e and i–E quadrants) covered the remaining 39.80% and accounted for 28.70% of total erosion. In the early stage (1995–2004), i–e, I–e, I–E and i–E areas accounted for an average of 31.31%, 33.33%, 29.80% and 5.56% of the watershed, respectively, indicating that approximately one-third of the basin combined high connectivity and high erosion. In the intermediate stage (2005–2014), the average proportion of i–e areas increased to 40.80%, whereas I–E areas decreased to 22.89%; I–e and i–E areas occupied 25.37% and 10.94%, respectively. In the late stage (2015–2020), i–e, I–e, I–E and i–E areas accounted for an average of 36.36%, 45.45%, 15.15% and 3.04%, respectively. Nevertheless, in 2020, the high-connectivity, high-erosion (I–E) areas still covered 18.67% of the watershed and contributed more than 40.00% of the total erosion. Overall, the results indicated that both erosion intensity and sediment connectivity in the Hantaichuan Watershed decreased significantly from 1995 to 2020.

4 Discussion

4.1 Spatio-temporal variations in erosion

The soil erosion modulus in the Hantaichuan Watershed exhibited significant spatio-temporal variations from 1995 to 2020, with a total reduction of 43.90%. This reduction was primarily

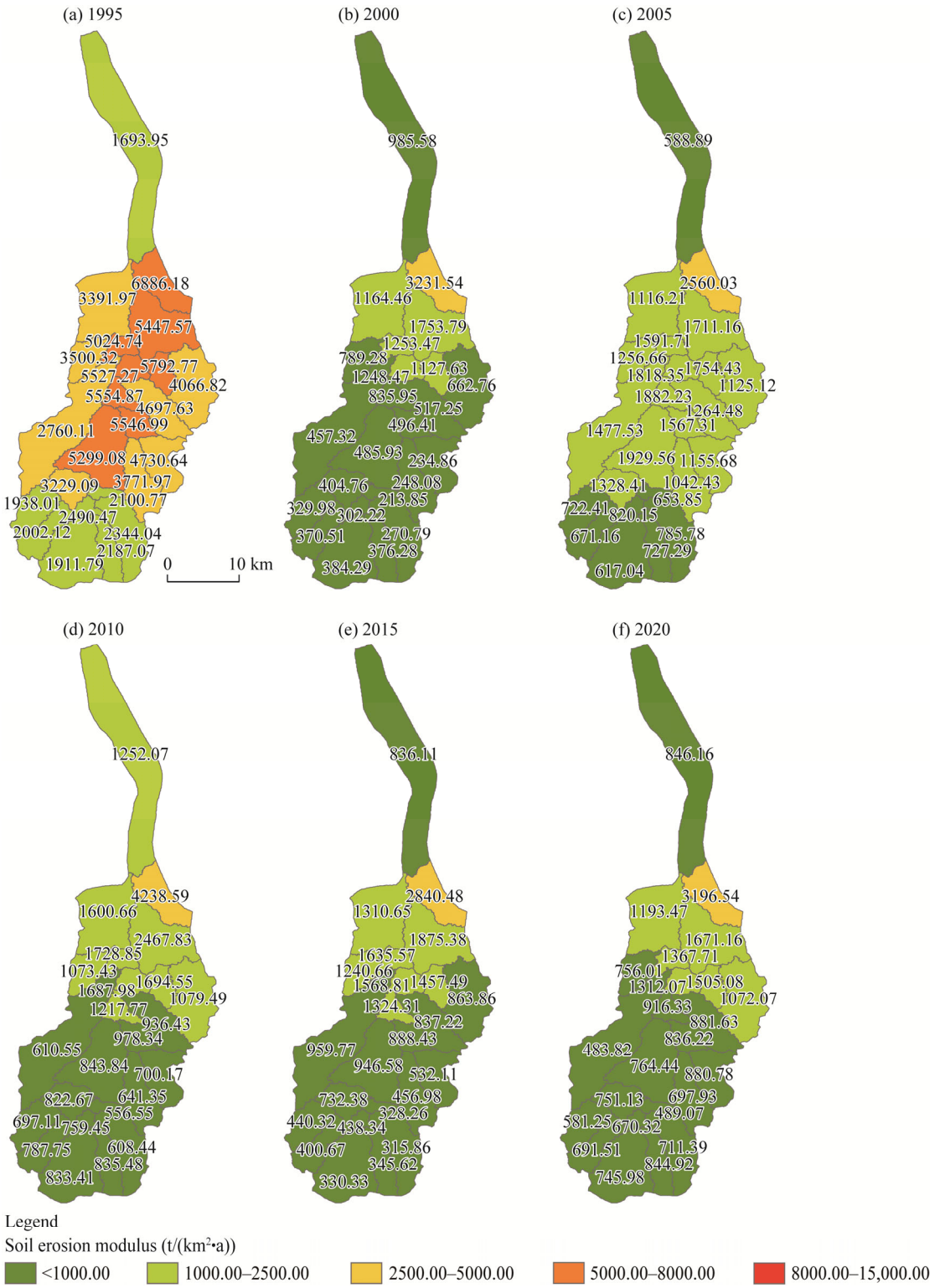

Fig. 7 Spatio-temporal change in soil erosion in the sub-basins of the Hantaichuan Watershed from 1995 to 2020. (a), 1995; (b), 2000; (c), 2005; (d), 2010; (e), 2015; (f), 2020.

driven by the substantial transformations in land use and associated changes in vegetation coverage, as shown in the variations in cover management factor and soil conservation practice

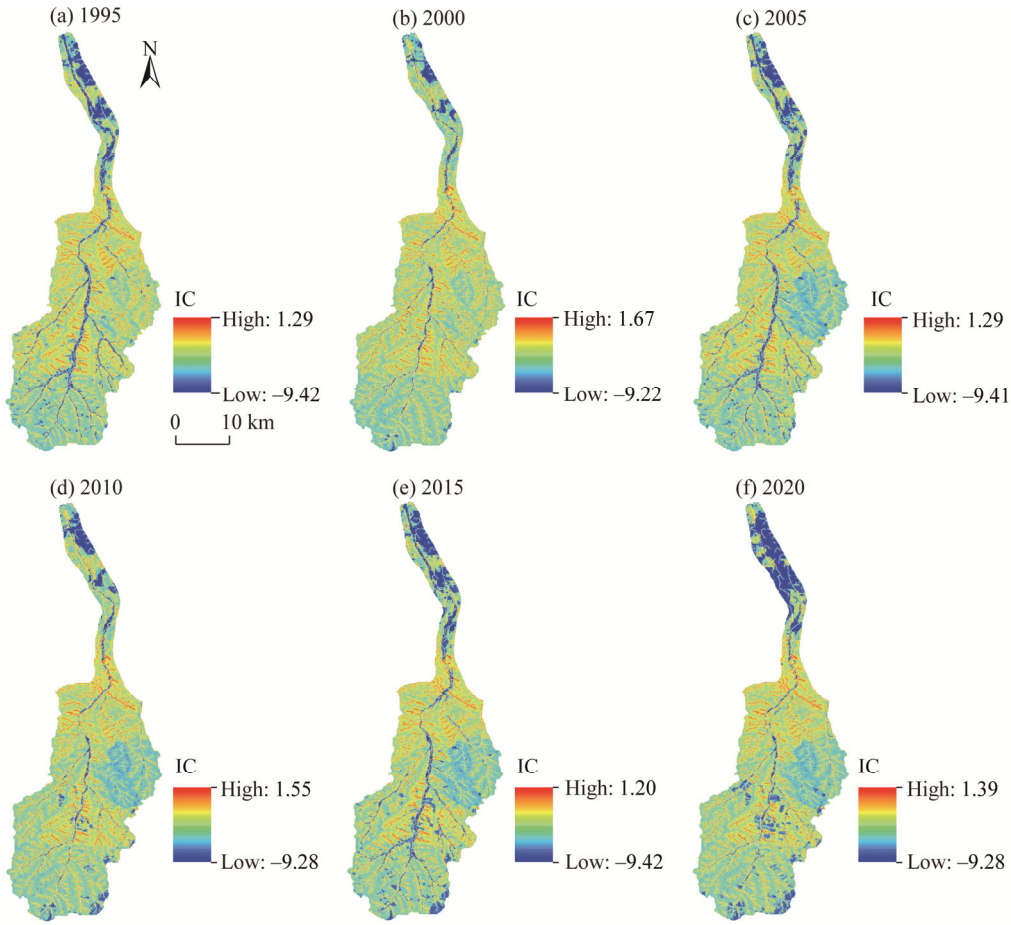

Fig. 8 Spatio-temporal change in IC in the Hantaichuan Watershed from 1995 to 2020. (a), 1995; (b), 2000; (c), 2005; (d), 2010; (e), 2015; (f), 2020.

factors (Chen et al., 2021; Moisa et al., 2021; Dash and Maity, 2023; Ferreira et al., 2024). Following the implementation of the "Grain for Green" Program and the regional grazing ban policy in Ordos City during the early 21st century, vast areas of sloping cropland and bare land were converted into grassland and shrubland (Bao, 2024). The increase in vegetation cover played a vital role in reducing soil erosion by intercepting rainfall kinetic energy, increasing surface roughness, and enhancing soil infiltration, which collectively reduced the detachment capacity of surface runoff (Guo et al., 2018; Shi et al., 2019; Zhao et al., 2020; Liu et al., 2021).

Spatially, the distribution of erosion remained highly heterogeneous. The high-intensity erosion was concentrated in the central part of the watershed, whereas low-intensity erosion occurred mainly in the northern and southern regions. This spatial pattern resulted primarily from the unique lithological and geomorphological conditions of the study area. The widespread exposure of Pisha sandstone in the central high-erosion zone, which is highly erodible upon contact with water, provided a persistent sediment source (Liu, 2023; Zhao, 2023). These findings aligned with studies in the adjacent Huangfuchuan watershed (Zhao et al., 2017), suggesting that vegetation restoration mitigates erosion, however, the lithology is the dominant factor in Pisha sandstone areas. Furthermore, aeolian sand transported from the adjacent Hobq Desert was frequently remobilized by hydrological processes, thus maintaining a high background erosion rate despite extensive vegetation restoration on the slopes. These findings emphasized the combined effect of lithology and vegetation recovery on long-term erosion dynamics, which should be carefully considered in future soil conservation and sediment management strategies.

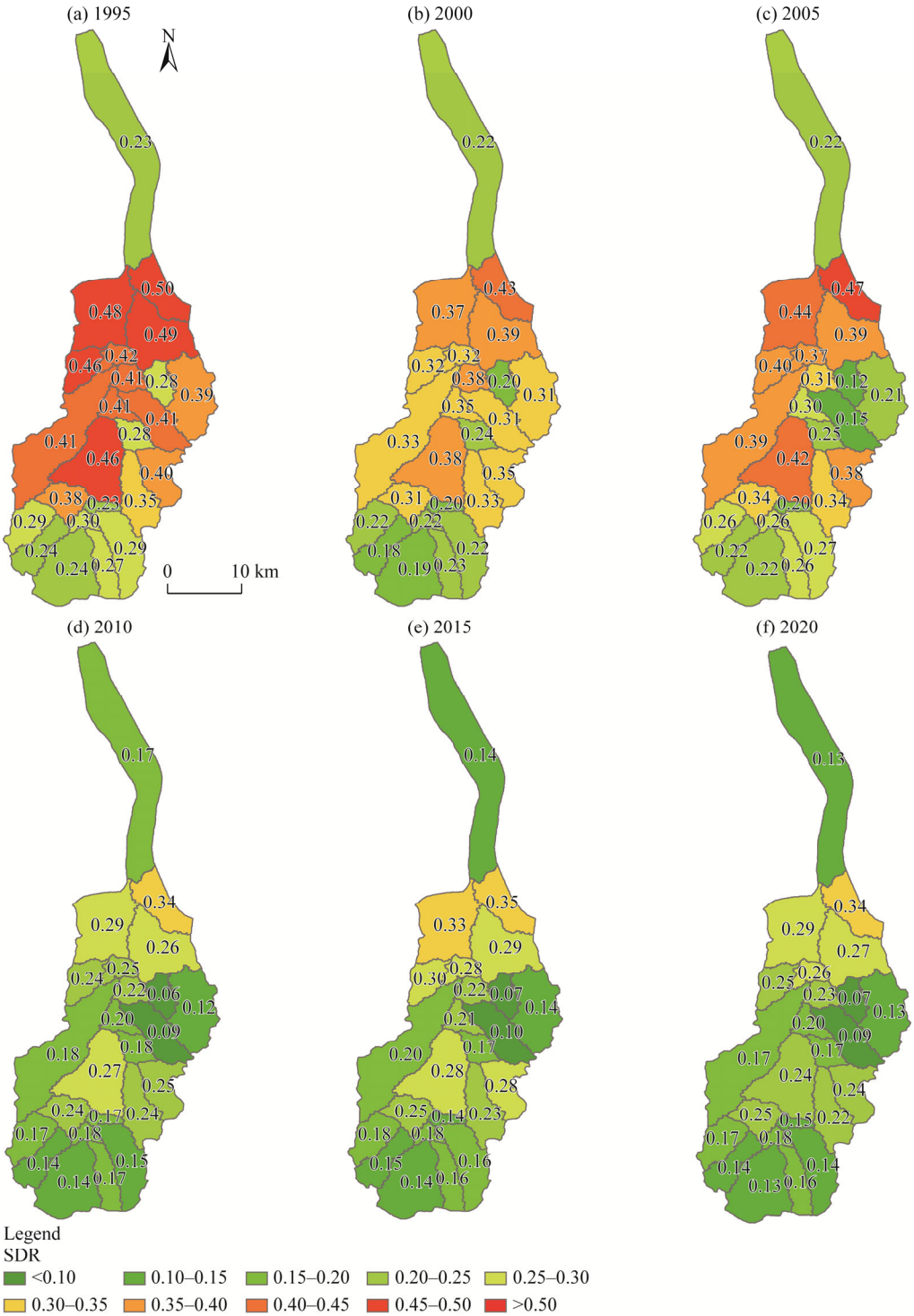

Fig. 9 Spatial distribution of SDR in the sub-basins of the Hantaichuan Watershed in 1995 (a), 2000 (b), 2005 (c), 2010 (d), 2015 (e), and 2020 (f)

4.2 Changes in sediment connectivity and sediment yield

To estimate sediment yield at watershed scale, we integrated RUSLE model with IC and SDR. Both the potential soil erosion rate and sediment yield decreased markedly over the study period;

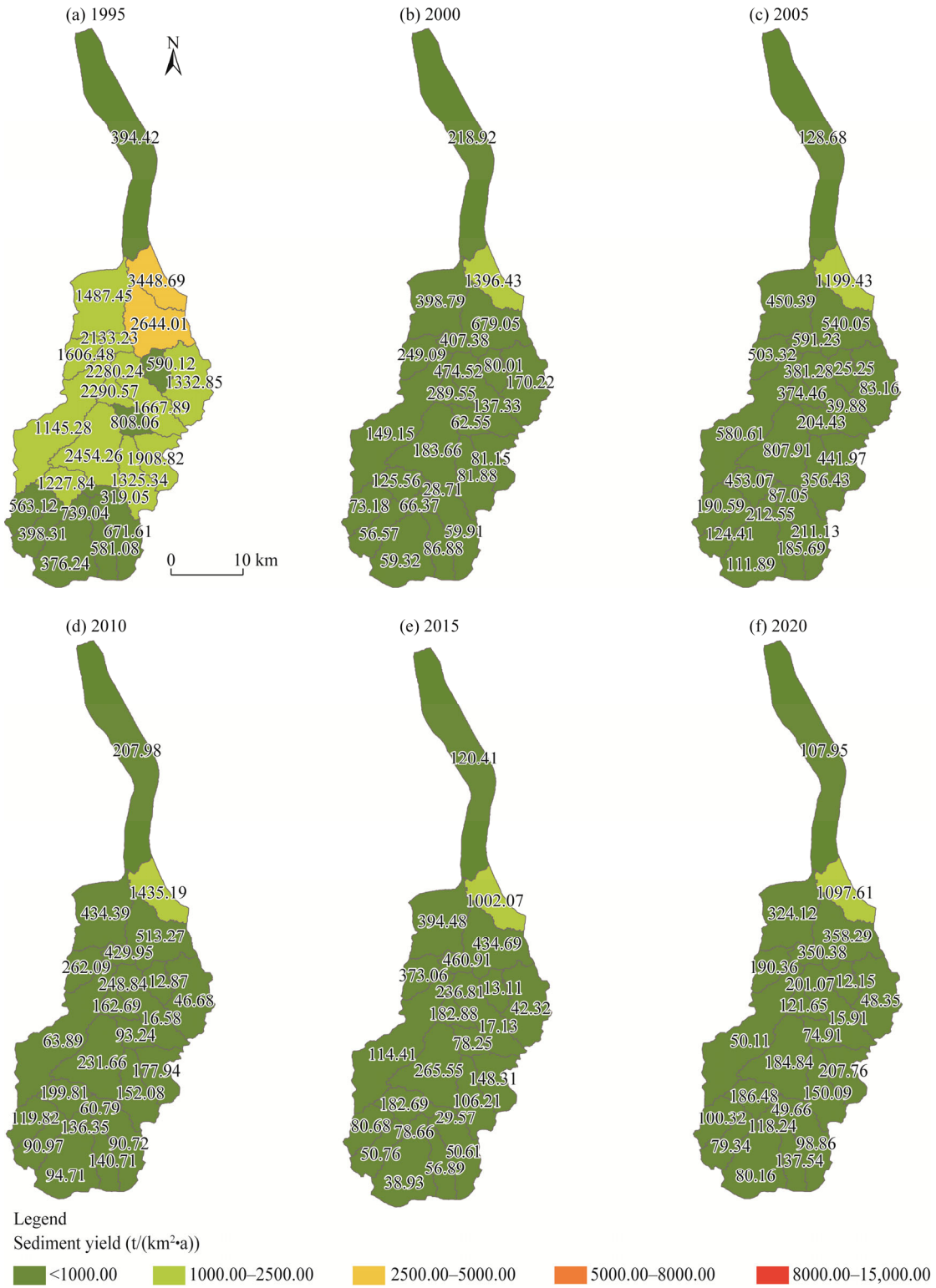

Fig. 10 Spatial distribution of simulated sediment yield with the trapping effects of check dams in the sub-basins in the Hantaichuan Watershed in 1995 (a), 2000 (b), 2005 (c), 2010 (d), 2015 (e), and 2020 (f)

however, sediment yield declined more strongly, with a reduction of 69.28% by 2020. This larger decline in off-site sediment yield relative to on-site erosion highlighted the critical regulatory role

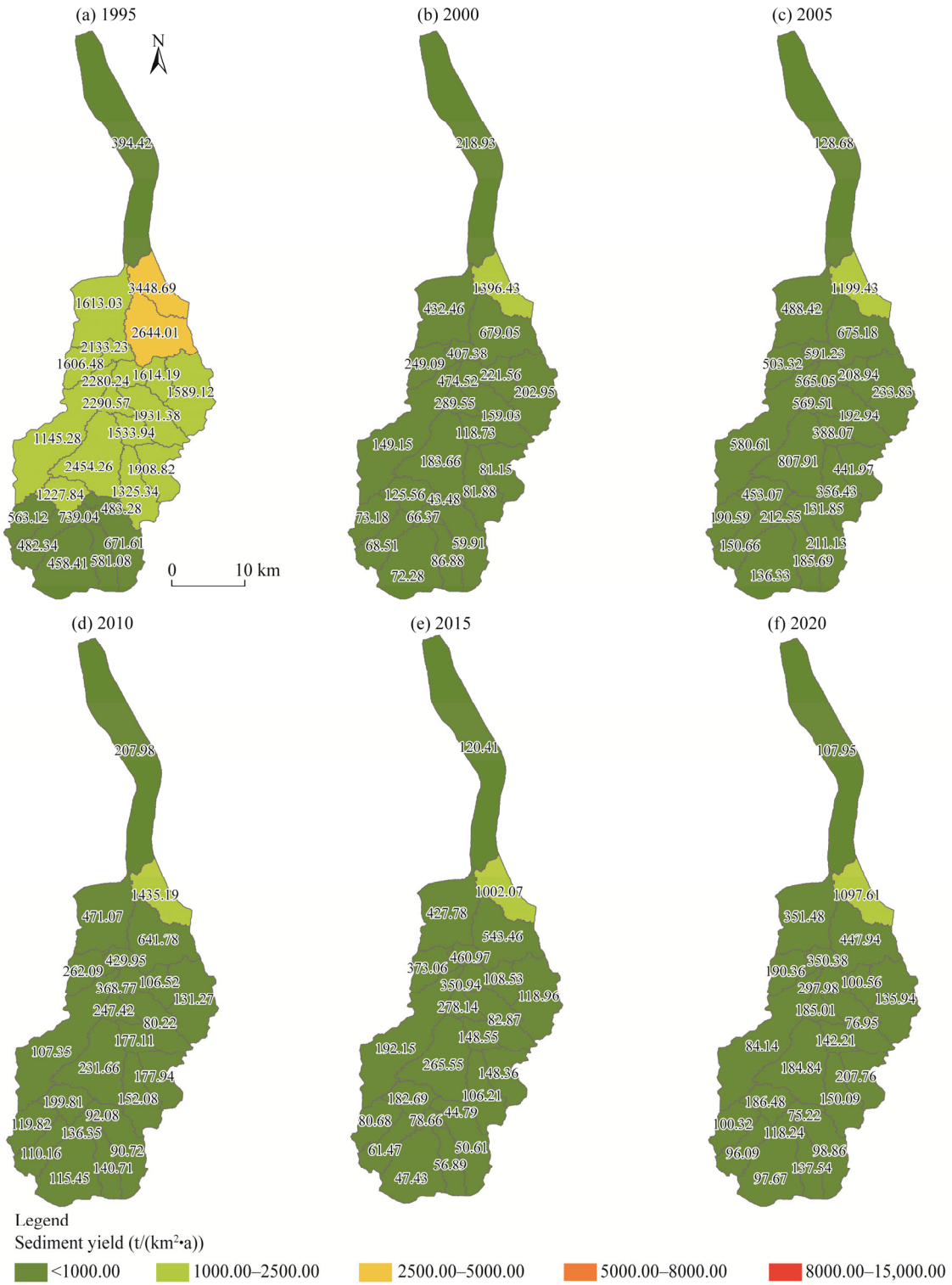

Fig. 11 Spatial distribution of estimated sediment yield in the sub-basins of the Hantaichuan Watershed in 1995 (a), 2000 (b), 2005 (c), 2010 (d), 2015 (e), and 2020 (f)

of sediment connectivity and SDR. Sediment connectivity is generally influenced by both topographic features (e.g., slope gradient and catchment area) and landscape allocation (e.g., land

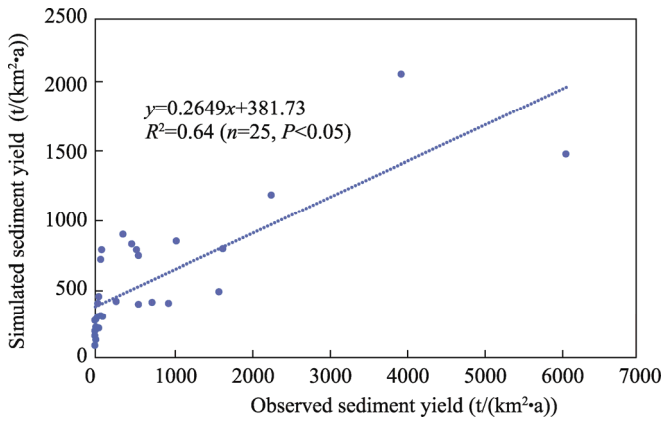

Fig. 12 Comparison between observed and simulated sediment yield at the Xiangshawan Hydrological Station from 1995 to 2020

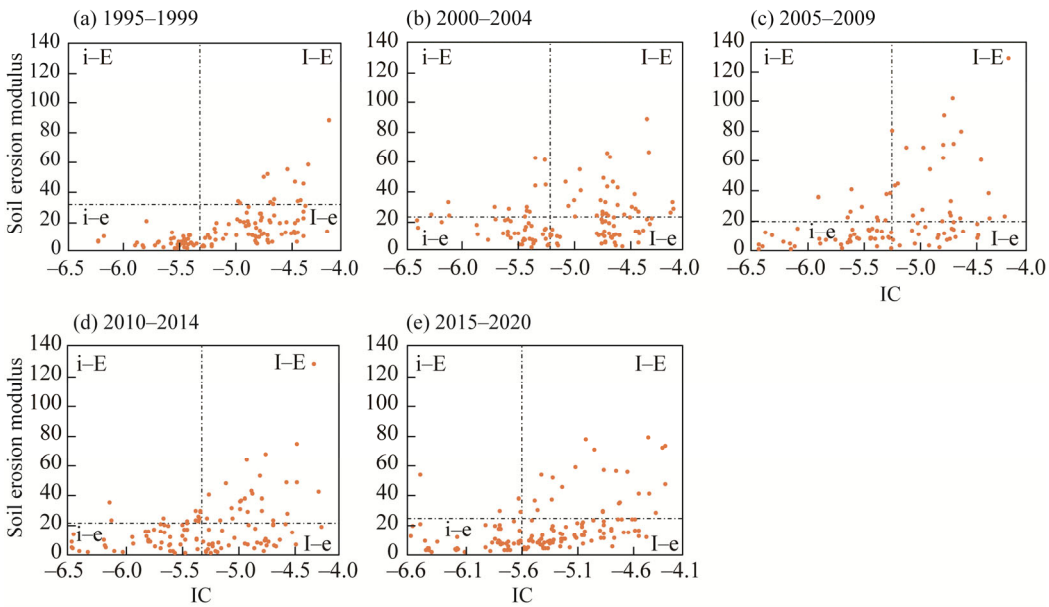

Fig. 13 IC–SE map of the Hantaichuan Watershed from 1995 to 2020. (a), 1995–1999; (b), 2000–2004; (c), 2005–2009; (d), 2010–2014; (e), 2015–2020. i–E represents low connectivity and high erosion; I–E represents high connectivity and high erosion; i–e represents low connectivity and low erosion; and I–e represents high connectivity and low erosion.

use and land cover) (Borselli et al., 2008; Diodato and Grauso, 2009; Baartman et al., 2013; Zuo et al., 2016). In the Hantaichuan Watershed, the results indicated that the sediment connectivity has decreased significantly over the past two decades, a phenomenon driven by the synergistic effects of ecological restoration and engineering measures.

The conversion of cropland and bare land into grassland and forest land enhanced surface roughness and improved soil structure and water retention capacity, thereby reducing flow energy and sediment mobility (Le Bissonnais et al., 2004; Appels et al., 2016; Sheng et al., 2025). As vegetation cover increased, root reinforcement and canopy interception further increased soil cohesion and surface protection, effectively reducing sediment detachment and sediment transport capacity (Pollen-Bankhead and Simon, 2010; Sandercock and Hooke, 2011). Moreover, the construction of check dams served as a decisive engineering intervention that physically disrupted sediment transport pathways (Shi et al., 2019; Zhao et al., 2020; Gu et al., 2021; Bai et al., 2023; Zeng et al., 2023). By comparing the scenarios with and without check dams, the results indicated

that though land use/cover changes were the dominant factor of sediment reduction on hillslopes, check dams acted as absolute sinks for the channel network, trapping large amount of sediment from upstream erosion areas. These structures disrupt sediment transport pathways, increase sediment deposition, and stabilize gullies and channels, thereby reducing sediment export from basin (Li et al., 2017; Zhao et al., 2017; Shi et al., 2019). By 2020, a total of 88 check dams had been constructed within the Hantaichuan Watershed, serving as critical structures for controlling gully erosion and stabilizing channel systems. Overall, the progressive reduction in sediment yield resulted from the synergistic effects of ecological restoration and engineering measures, both of which effectively disrupted sediment transfer pathways and improved sediment retention.

4.3 Covariations between sediment connectivity and soil erosion

Understanding the spatial correspondence between sediment connectivity and soil erosion is essential for identifying the dominant sediment transfer mechanisms in watersheds. The analysis of the IC–SE maps revealed both coupling (high–high or low–low) and decoupling (high–low or low–high) covariations between sediment connectivity and soil erosion. The identification of I-E zones provides a precise delineation of critical source areas. Although these I–E zones covered only 18.67% of the total watershed area, that contributed disproportionately to the sediment budget, accounting for over 40.00% of the total erosion. These areas typically corresponded to the steep and Pisha sandstone-dominated gullies where vegetation establishment is challenging. This spatial concentration agreed with previous findings by Michalek et al. (2021) and Guo et al. (2023), who reported that a small fraction of I–E zones contributed disproportionately to the total sediment load. These findings emphasized that effective sediment management should prioritize these critical source areas, as localized interventions in the I–E zones can substantially reduce overall sediment yield and improve watershed sustainability.

Conversely, the analysis also revealed a decoupling phenomenon, specifically in the low-connectivity and high-erosion (i–E) zones. Contrary to previous assumption that such decoupling might be caused by natural blockages like landslides (Vigiak et al., 2016; Zhang, 2019; Liu et al., 2022), this pattern was largely attributable to anthropogenic interception in the Hantaichuan Watershed. High-erosion slopes located immediately upstream of check dams or far from the drainage network fail to deliver their sediment load effectively to the outlet, resulting in high local erosion but low contribution to the watershed sediment yield. These findings suggested a paradigm shift for future conservation strategy: management resources should be prioritized for the I–E zones, which represent critical source areas, rather than being uniformly distributed across the watershed. For these critical areas, more aggressive bio-engineering measures, such as sea-buckthorn flexible dams or high-durability engineering structures, are required to stabilize the Pisha sandstone. Meanwhile, for the i–E zones, the strategy should focus on the maintenance of existing check dams to prevent the reconnexion of stored sediment due to dam failure or filling.

4.4 Model uncertainties

Despite the robust framework established in this study, several uncertainties and limitations must be acknowledged. Uncertainties within the modeling framework mainly arose from limitations in the input data and simplifications in the model structure. The rainfall erosivity factor, which was interpolated from a limited number of meteorological stations, may have caused underestimation of spatial heterogeneity, particularly during extreme rainfall events in arid areas. Similarly, the sediment retention effect of check dams was represented by a static coefficient, which does not account for temporal variations as reservoirs gradually filled with sediment, thereby potentially biasing the estimated sediment yield. Notably, RUSLE model has been primarily used to estimate hillslope erosion and does not account for gully erosions, which are known to be significant sediment sources on the Loess Plateau (Renard et al., 1997; Li et al., 2020; Zhao et al., 2020). However, the calibration of the SDR module using observed sediment yield data partially compensates for this limitation by adjusting the total sediment export volume to match reality (Zhao et al., 2020).

Another key source of uncertainty concerned the representation of sediment connectivity. The present study employed a structural sediment connectivity framework, which characterized connectivity in consideration of topography, flow paths, and impedance factors (Zhao et al., 2020; Liu et al., 2021; Guo et al., 2023). However, recent studies have emphasized the importance of functional connectivity, which reflects the dynamic hydro-sedimentological processes influencing sediment transfer (Cavalli et al., 2019). For example, Zanandrea et al. (2021) analyzed the spatio-temporal variability in sediment transport pathways during heavy rainfall events by developing a hydro-sedimentological connectivity index. Structural connectivity reflects the static transport potential of geomorphic units, whereas functional connectivity captures the dynamic response of runoff–erosion processes. These two processes play different dominant roles at different spatio-temporal scales (Najafi et al., 2021). Therefore, future studies on sediment connectivity at the watershed scale should integrate event-based functional indicators of rainfall, runoff, and sediment fluxes, for example by coupling IC with hydro-sedimentological or modified connectivity indices that combine structural and functional components (Zanandrea et al., 2021; Liu et al., 2022). Such approaches, which jointly represent structural and functional connectivity and are supported by targeted field monitoring, would provide a more realistic representation of sediment delivery dynamics across spatial and temporal scales.

5 Conclusions

This study focused on the spatio-temporal variations in soil erosion and sediment yield in the Hantaichuan Watershed from 1995 to 2020, and changes in the relationship between soil erosion and sediment connectivity. From 1995 to 2020, the increase in grassland area, and the marked decrease in bare land area significantly reduced the soil erosion modulus by 43.90%. These land use/cover changes significantly decreased both IC and SDR values, with land use/cover changes alone led to a 63.60% decrease in sediment yield, whereas the combined effect of land use/cover changes and check dam construction resulted in an overall 69.28% reduction in sediment yield. An analysis of the IC–SE maps revealed both coupling and decoupling covariations. Specifically, the "high connectivity and high erosion" (I–E) zones, primarily located in the central part of the watershed (sub-basins 2, 3, 5, and 7), were identified as critical source areas. Although these areas covered only 18.67% of the watershed, they contributed more than 40.00% to the total erosion. Therefore, future conservation measures should prioritize these specific hotspots to maximize sediment reduction efficiency.

Conflicts of interest

The authors declare that they have no known competing financial interests or personal relationships that could have appeared to influence the work reported in this paper.

Acknowledgements

This study was supported by the National Natural Science Foundation of China (42077076, 42177323) and the National Natural Science Foundation of China and Yellow River Water Science Research Joint Fund (U2243211). The authors would like to express their great gratitude to the Hydrological Station in the Hantaichuan Watershed for collecting suspended sediment samples during the flood events. The authors would also like to thank the reviewers for the very valuable comments, which greatly improved the quality of the paper.

Author contributions

Conceptualization: ZHAO Guangju; Data curation: SHAN Rui, ZHAO Guangju, TIAN Peng, GUO Xiaoxue, LU Ang; Methodology: SHAN Rui, ZHAO Guangju, MU Xingmin, LU Ang; Investigation: SHAN Rui, LU Ang, FAN Junjian, ZHAO Yanbo; Formal analysis: SHAN Rui, LU Ang; Writing - original draft preparation: SHAN Rui; Writing - review and editing: SHAN Rui, ZHAO Guangju, MU Xingmin, TIAN Peng; Funding acquisition: ZHAO

Guangju; Resources: ZHAO Guangju; Supervision: ZHAO Guangju, TIAN Peng; Project administration: ZHAO Guangju; Software: SHAN Rui, LU Ang, ZHAO Yanbo, FAN Junjian, GUO Xiaoxue; Validation: SHAN Rui; Visualization: SHAN Rui, TIAN Peng. All authors approved the manuscript.

References

Abebe N, Eekhout J, Vermeulen B, et al. 2023. The potential and challenges of the 'RUSLE-IC-SDR' approach to identify sediment dynamics in a Mediterranean catchment. CATENA, 233: 107480, doi: 10.1016/j.catena.2023.107480.

Appels W M, Bogaart P W, van der Zee S E A T M. 2016. Surface runoff in flat terrain: How field topography and runoff generating processes control hydrological connectivity. Journal of Hydrology, 534: 493–504.

Arnold J G, Srinivasan R, Muttiah J R, et al. 1998. Large area hydrologic modeling and assessment Part 1: model development. Journal of the American Water Resources Association, 34(1): 73–89.

Baartman J E M, Masselink R, Keesstra S D, et al. 2013. Linking landscape morphological complexity and sediment connectivity. Earth Surface Processes and Landforms, 38(12): 1457–1471.

Bai L L, Shi P, Wang W, et al. 2023. Sediment sources and their impacts on a check dam-controlled watershed, Loess Plateau, China. Journal of Mountain Science, 20: 1660–1673.

Bao Y T. 2024. An analysis of land-use change and driving force in Ordos. Geographical Science Research, 13(1): 82156, doi: 10.12677/GSER.2024.131023. (in Chinese)

Bhattacharya R K, Das Chatterjee N, Das K. 2024. Modelling of soil erosion susceptibility incorporating sediment connectivity and export at landscape scale using integrated machine learning, InVEST-SDR and Fragstats. Journal of Environmental Management, 353: 120164, doi: 10.1016/j.jenvman.2024.120164.

Borselli L, Cassi P, Torri D. 2008. Prolegomena to sediment and flow connectivity in the landscape: A GIS and field numerical assessment. CATENA, 75(3): 268–277.

Bracken L J, Croke J. 2007. The concept of hydrological connectivity and its contribution to understanding runoff-dominated geomorphic systems. Hydrological Processes, 21(13): 1749–1763.

Brune G M. 1953. Trap efficiency of reservoirs. Eos, Transactions American Geophysical Union, 34(3): 407–418.

Cai C F, Ding S W, Shi Z H, et al. 2000. Study of applying USLE and geographical information system IDRISI to predict soil erosion in small watershed. Journal of Soil and Water Conservation, 14(2): 19–24. (in Chinese)

Cavalli M, Trevisani S, Comiti F, et al. 2013. Geomorphometric assessment of spatial sediment connectivity in small Alpine catchments. Geomorphology, 188: 31–41.

Cavalli M, Vericat D, Pereira P. 2019. Mapping water and sediment connectivity. Science of the Total Environment, 673: 763–767.

Chen J, Li Z W, Xiao H B, et al. 2021. Effects of land use and land cover on soil erosion control in southern China: Implications from a systematic quantitative review. Journal of Environmental Management, 282: 111924, doi: 10.1016/j.jenvman.2020.111924.

Dash S S, Maity R. 2023. Effect of climate change on soil erosion indicates a dominance of rainfall over LULC changes. Journal of Hydrology: Regional Studies, 47: 101373, doi: 10.1016/j.ejrh.2023.101373.

Diodato N, Grauso S. 2009. An improved correlation model for sediment delivery ratio assessment. Environmental Earth Sciences, 59: 223–231.

Fan S H, Qin F C, Che Z H. 2024. Geochemical indicators to constrain weathering, provenance and tectonic setting of the Pisha Sandstone (Early–Middle Triassic) in Northeast Ordos Basin, China. Heliyon, 10(8): e29120, doi: 10.1016/j.heliyon.2024.e29120.

Ferreira C S S, Kašanin-Grubin M, Kapović Solomun M, et al. 2024. Chapter 13 – Impacts of land use and land cover changes on soil erosion. In: Melesse A M, Rahmati O, Khosravi K, et al. Remote Sensing of Soil and Land Surface Processes. Monitoring, Mapping, and Modeling. Amsterdam: Elsevier, 229–248.

Fu B J, Liu Y, Lü Y H, et al. 2011. Assessing the soil erosion control service of ecosystems change in the Loess Plateau of China. Ecological Complexity, 8(4): 284–293.

Ganasri B P, Ramesh H. 2016. Assessment of soil erosion by RUSLE model using remote sensing and GIS—A case study of Nethravathi Basin. Geoscience Frontiers, 7(6): 953–961.

Gu C J, Zhu Y Q, Li R H, et al. 2021. Effects of different soil and water conservation measures on hydrological extremes and flood processes in the Yanhe River, Loess Plateau, China. Natural Hazards, 109: 545–566.

Guo S S, Zhu Z R, Lü L. 2018. Effects of climate change and human activities on soil erosion in the Xihe River Basin, China. Water, 10(8): 1085, doi: 10.3390/w10081085.

Guo Z J, Wu L, Liu S, et al. 2023. An integrated watershed modeling framework to explore the covariation between sediment connectivity and soil erosion. European Journal of Soil Science, 74(5): 13412, doi: 10.1111/ejss.13412.

Hamel P, Falinski K, Sharp R, et al. 2017. Sediment delivery modeling in practice: Comparing the effects of watershed characteristics and data resolution across hydroclimatic regions. Science of the Total Environment, 580: 1381–1388.

Hao R, Huang X, Cai Z W, et al. 2022. Incorporating sediment connectivity index into MUSLE model to explore soil erosion and sediment yield relationships at event scale. Journal of Hydrology, 614: 128579, doi: 10.1016/j.jhydrol.2022.128579.

Jain M K, Kothyari U C. 2000. Estimation of soil erosion and sediment yield using GIS. Hydrological Sciences Journal, 45(5): 771–786.

Jenks G F. 1967. The data model concept in statistical mapping. In: International Yearbook of Cartography. Gutersloh: C. Bertelsman Verlag, 186–190.

Le Bissonnais Y, Lecomte V, Cerdan O. 2004. Grass strip effects on runoff and soil loss. Agronomy for Sustainable Development, 24(3): 129–136.

Li E H, Mu X M, Zhao G J, et al. 2017. Effects of check dams on runoff and sediment load in a semi-arid river basin of the Yellow River. Stochastic Environmental Research and Risk Assessment, 31: 1791–1803.

Li J L, Sun R H, Xiong M Q, et al. 2020. Estimation of soil erosion based on the RUSLE model in China. Acta Ecologica Sinica, 40(10): 3473–3485. (in Chinese)

Liu C X, Chen Y N, Fang G H, et al. 2024. Impact of climatic and geomorphologic drivers on sediment connectivity in the Tarim River Basin, China. Journal of Hydrology, 643: 132027, doi: 10.1016/j.jhydrol.2024.132027.

Liu S. 2024. Analysis of factors affecting sediment connectivity and simulation of sediment production in the Jinghe River Basin. MSc Thesis. Yangling: Northwest A&F University. (in Chinese)

Liu W, Shi C X, Ma Y Y, et al. 2021. Land use and land cover change-induced changes of sediment connectivity and their effects on sediment yield in a catchment on the Loess Plateau in China. CATENA, 207: 105688, doi: 10.1016/j.catena.2021.105688.

Liu W, Shi C X, Ma Y Y, et al. 2022. Evaluating sediment connectivity and its effects on sediment reduction in a catchment on the Loess Plateau, China. Geoderma, 408: 115566, doi: 10.1016/j.geoderma.2021.115566.

Liu X R, Feng T J, Zhang Y F, et al. 2025. Vegetation restoration affects soil hydrological processes in typical natural and planted forests on the Loess Plateau. Journal of Hydrology, 650: 132465, doi: 10.1016/j.jhydrol.2024.132465.

Liu Z T. 2023. Runoff and sediment changes and their responses to precipitation and land use change in Hantaichuan Watershed. MSc Thesis. Hohot: Inner Mongolia Agricultural University. (in Chinese)

López-Vicente M, Poesen J, Navas A, et al. 2013. Predicting runoff and sediment connectivity and soil erosion by water for different land use scenarios in the Spanish Pre-Pyrenees. CATENA, 102: 62–73.

Luo D. 2022. Eco-hydrological effects of different vegetation restoration catchments in the gully region of Loess Plateau. PhD Dissertation. Xi'an: Institute of Earth Environment, Chinese Academy of Sciences. (in Chinese)

Michalek A, Zarnaghsh A, Husic A. 2021. Modeling linkages between erosion and connectivity in an urbanizing landscape. Science of the Total Environment, 764: 144255, doi: 10.1016/j.scitotenv.2020.144255.

Millares-Valenzuela A, Eekhout J P C, Martínez-Salvador A, et al. 2022. Evaluation of sediment connectivity through physically-based erosion modeling of landscape factor at the event scale. CATENA, 213: 106165, doi: 10.1016/j.catena.2022.106165.

Min J, Liu X H, Li H Y, et al. 2024. Spatio-temporal variations in soil erosion and its driving forces in the Loess Plateau from 2000 to 2050 based on the RUSLE model. Applied Sciences, 14(13): 5945, doi: 10.3390/app14135945.

Ministry of Water Resources of the People's Republic of China. 1995–2020. Hydrological Yearbook of the People's Republic of China: Hydrological Data of the Yellow River Basin. Beijing: China Water & Hydropower Press. (in Chinese)

Ministry of Water Resources of the People's Republic of China. 2008. Standard for Classification and Gradation of Soil Erosion (SL 190–2007). [2025-05-04]. https://www.mwr.gov.cn/. (in Chinese)

Moisa M B, Negash D A, Merga B B, et al. 2021. Impact of land-use and land-cover change on soil erosion using the RUSLE model and the geographic information system: a case of Temeji Watershed, western Ethiopia. Journal of Water and Climate Change, 12(7): 3404–3420.

Najafi S, Dragovich D, Heckmann T, et al. 2021. Sediment connectivity concepts and approaches. CATENA, 196: 104880, doi: 10.1016/j.catena.2020.104880.

Persichillo M G, Bordoni M, Cavalli M, et al. 2018. The role of human activities on sediment connectivity of shallow landslides. CATENA, 160: 261–274.

Pinzon J E, Pak E W, Tucker C J, et al. 2023. Global Vegetation Greenness (NDVI) from AVHRR GIMMS-3G+, 1981–2022. [2025-05-23]. https://www.earthdata.nasa.gov/data/catalog/ornl-cloud-global-veg-greenness-gimms-3g-2187-1#overview=.

Pollen-Bankhead N, Simon A. 2010. Hydrologic and hydraulic effects of riparian root networks on streambank stability: Is mechanical root-reinforcement the whole story? Geomorphology, 116(3–4): 353–362.

Renard K G, Foster G R, Weesies G A, et al. 1997. Predicting soil erosion by water: A guide to conservation planning with the Revised Universal Soil Loss Equation (RUSLE). In: The United States Department of Agriculture (USDA) Agriculture

Handbook No. 703. Washington D.C.: USDA, 45–65.

Sandercock P J, Hooke J M. 2011. Vegetation effects on sediment connectivity and processes in an ephemeral channel in SE Spain. Journal of Arid Environments, 75(3): 239–254.

Sheng F, Yi T X, Wang Y Y, et al. 2025. Changes in sediment connectivity and its impact on sediment transport in a typical watershed of southern Jiangxi Province, China. Ecological Indicators, 171: 113204, doi: 10.1016/j.ecolind.2025.113204.

Shi P, Zhang Y, Ren Z Q, et al. 2019. Land-use changes and check dams reducing runoff and sediment yield on the Loess Plateau of China. Science of the Total Environment, 664: 984–994.

Stephens C M, Lall U, Johnson F M, et al. 2021. Landscape changes and their hydrologic effects: Interactions and feedbacks across scales. Earth-Science Reviews, 212: 103466, doi: 10.1016/j.earscirev.2020.103466.

Sun W Y, Shao Q Q, Liu J Y, et al. 2014. Assessing the effects of land use and topography on soil erosion on the Loess Plateau in China. CATENA, 121: 151–163.

Tang C J, Liu Y, Li Z W, et al. 2021. Effectiveness of vegetation cover pattern on regulating soil erosion and runoff generation in red soil environment, southern China. Ecological Indicators, 129: 107956, doi: 10.1016/j.ecolind.2021.107956.

Thapa P. 2020. Spatial estimation of soil erosion using RUSLE modeling: a case study of Dolakha District, Nepal. Environmental Systems Research, 9: 15, doi: 10.21203/rs.3.rs-25478/v4.

Vigiak O, Borselli L, Newham L T H, et al. 2012. Comparison of conceptual landscape metrics to define hillslope-scale sediment delivery ratio. Geomorphology, 138(1): 74–88.

Vigiak O, Beverly C, Roberts A, et al. 2016. Detecting changes in sediment sources in drought periods: The Latrobe River case study. Environmental Modelling & Software, 85: 42–55.

Wang J H, Zhang R G, Sun J. 2018. Experimental study on influence of vegetation coverage on runoff in wind-water erosion crisscross region. Earth and Environmental Science, 121(12): 022021, doi: 10.1088/1755-1315/121/2/022021.

Wischmeier W H, Smith D D. 1978. Predicting rainfall erosion losses: a guide to conservation planning. In: USDA Agriculture Handbook No. 537. Washington D.C.: USDA.

Woznicki S A, Cada P, Wickham J, et al. 2020. Sediment retention by natural landscapes in the conterminous United States. Science of the Total Environment, 745(25): 140972, doi: 10.1016/j.scitotenv.2020.140972.

Wuepper D, Borrelli P, Finger R. 2020. Countries and the global rate of soil erosion. Nature Sustainability, 3: 51–55.

Yang H, Shi C X. 2018. Spatial and temporal variations of aeolian sediment input to the tributaries (the Ten Kongduis) of the upper Yellow River. Aeolian Research, 30: 1–10.

Yang K, Zhang J T, Cui D G, et al. 2025. Multi-scale study of the synergy between human activities and climate change on urban heat islands in China. Sustainable Cities and Society, 125: 106341, doi: 10.1016/j.scs.2025.106341.

Zanandrea F, Michel G P, Kobiyama M, et al. 2019. Evaluation of different DTMs in sediment connectivity determination in the Mascarada River Watershed, southern Brazil. Geomorphology, 332: 80–87.

Zanandrea F, Michel G P, Kobiyama M, et al. 2021. Spatial-temporal assessment of water and sediment connectivity through a modified connectivity index in a subtropical mountainous catchment. CATENA, 204: 105380, doi: 10.1016/j.catena.2021.105380.

Zeng W Y, Tian Y S, Zhai J, et al. 2025. Soil erosion resilience under climate extremes: Disentangling the impacts of vegetation restoration and rainfall intensification across China. Ecological Indicators, 178: 113994, doi: 10.1016/j.ecolind.2025.113994.

Zeng Y, Meng X D, Wang B, et al. 2023. Effects of soil and water conservation measures on sediment delivery processes in a hilly and gully watershed. Journal of Hydrology, 616: 128804, doi: 10.1016/j.jhydrol.2022.128804.

Zhang T, Peng J, Liang W, et al. 2016. Spatial-temporal patterns of water use efficiency and climate controls in China's Loess Plateau during 2000–2010. Science of the Total Environment, 565: 105–122.

Zhang W B, Fu J S. 2003. Rainfall erosivity estimation under different rainfall amount. Resources Science, 25(1): 35–41. (in Chinese)

Zhang Y F. 2019. Response of channel sediment connectivity to channel morphology and rainfall in small watershed of the hill and gully Loess Plateau region. MSc Thesis. Yangling: Northwest A&F University. (in Chinese)

Zhang Y J. 2024. Study on the spatial-temporal evolution and potential risks of soil erosion in the Xiliugou Watershed of the Shi Da Kong Dui. MSc Thesis. Yangling: Northwest A&F University. (in Chinese)

Zhao G J, Kondolf G M, Mu X M, et al. 2017. Sediment yield reduction associated with land use changes and check dams in a catchment of the Loess Plateau, China. CATENA, 148: 126–137.

Zhao G J, Gao P, Tian P, et al. 2020. Assessing sediment connectivity and soil erosion by water in a representative catchment on the Loess Plateau, China. CATENA, 185: 104284, doi: 10.1016/j.catena.2019.104284.

Zhao J T. 2023. Response of soil erosion and water and sediment to land use change in the Hantaichuan Basin. MSc Thesis. Yangling: Northwest A&F University. (in Chinese)

Zuo D P, Xu Z X, Yao W Y, et al. 2016. Assessing the effects of changes in land use and climate on runoff and sediment yields from a watershed in the Loess Plateau of China. Science of the Total Environment, 544: 238–250.